Microstructure based model for sound absorption predictions of perforated closed-cell metallic foams

F. Chevillotte, Camille Perrot, R. Panneton

ICSV 17
THE 17th INTERNATIONAL CONGRESS ON SOUND & VIBRATION
CAIRO 18 - 22 JULY, 2010

MICROSTRUCTURE BASED MODEL FOR SOUND ABSORPTION PREDICTIONS OF PERFORATED CLOSED-CELL METALLIC FOAMS

Fabien Chevillotte, Raymond Panneton

GAUS, Department of mechanical engineering, Université de Sherbrooke (Qc), Canada, J1K 2R1

Camille Perrot

Université Paris-Est, Laboratoire Modélisation et Simulation Multi Echelle, MSME UMR 8208 CNRS, 5 bd Descartes, 77454 Marne-la-Vallée, France
e-mail: camille.perrot@univ-paris-est.fr

Closed-cell metallic foams are known for their rigidity, their lightness, their thermal conductivity as well as their low production cost compared to open-cell metallic foams. Yet, they are also poor sound absorbers. A method to enhance their sound absorption is to perforate them. This method has shown good preliminary results but has not yet been analyzed from a microstructural point of view. The objective of this work is to better understand how perforations modify the sound absorption of closed-cell metallic foams. First, a simple two-dimensional (2D) microstructural model of the perforated closed-cell metallic foam is proposed and solved through numerical homogenization. A rough three-dimensional (3D) correction of the 2D results is then given from the standpoint of straightforward examination of the analytical slits/cylinders macroscopic parameters. The results show that the diameter of both the perforation and the pore appear as the main controlling parameters of the sound absorption behavior. An experimental comparison demonstrates that the 2D proposed microstructural numerical model combined with a 3D analytical correction factor yields realistic trends for optimization purposes.

1. Introduction

How do local geometry parameters relate to sound absorption spectrum in perforated closed-cell metallic foams and how it compares to perforated rigid solids? This question arises with the continuously increasing interest of metallic foams combined attractive properties [1]. Recently, the study of sound absorption enhancement of closed-cell metallic foams, especially its relation to the

microstructure of a porous medium, was the focus of much attention. Among the various results of these studies, it was found that (1) techniques based on either rolling or hole drilling are resulting in sound absorption enhancement [2][3], and (2) progress can be made in the understanding of their normal sound absorption properties in relation with their local geometry parameters [4]. The purpose of this work is to carry out a trend analysis to clarify the microphysical foundations of the sound absorption of perforated closed-cell metallic foams and how it compares to perforated rigid solids. In this paper, the focus is on the long-wavelength acoustic behavior of perforated closed-cell metallic foams. Thus, a microstructural model which is not limited to uniform tubes of arbitrary cross section-shapes, but rather based on an array of spherical pores connected by perforations has to be developed. This work extends the PUC microstructural approach to better understand and quantify the effects of perforations in closed-cell metallic foams on the enhancement of sound absorption. In particular, a parametric study will focus on five local geometry descriptors: the perforation diameter D_{hole}, the perforation density n, the distance between spherical pores d, the relative position between spherical pores and perforations w, and the pore diameter a.

2. Materials and method

2.1 Local geometry model of perforated closed-cell metallic foams

A typical closed-cell aluminum foam is shown in Fig. 1. Such a foam can be modeled as a pack of air-filled spherical pores. Contrary to open-cell foams, this pack does not form an interconnected network of pores opened to the surrounding free-fluid medium. Consequently, an acoustic P2 compressional wave cannot penetrate and propagate in the fluid phase to dissipate its energy through visco-inertial forces (i.e., there is no relative motion between the frame and the air filling the pores). Such metallic foams are poor sound absorbers. With the aim of improving sound absorption of closed-cell metallic foams, one needs to promote relative motion between the frame and the saturating fluid by drilling holes through the closed-cell medium. The perforations are opened to the surrounding air and interconnect with some cells as depicted in black for a single perforation in Fig. 1 (left). On this real aluminum foam sample, one easily realizes that the pores may be interconnected differently depending on the position of the perforation. A priori, the way the pores are interconnected through the perforation may influence the velocity field patterns through the network and, as a consequence, the acoustical performances. To simplify the analysis, a local geometry having a regular repartition of monodispersed pores is firstly considered. This is shown in Fig. 1 (center). In this model, five characteristic parameters define the local geometry configuration: the diameter of the pores a, the diameter of perforations D_{hole}, the distance between pores d, the relative position between pores and perforations w, and the position of perforations. Here, two typical configurations of perforations are studied: (1) pores lined up with the perforation, and (2) pores alternated along the perforation. For each local configuration, the fluid domain is Ω_f, the fluid-solid interface is $\partial\Omega$, and the total periodic homogenization volume (containing both the solid and fluid phases) is shown by the dashed lines. Note that the input surface of each configuration is characterized by a surface porosity given by $h_s = D_{hole}/H_i$ with $i = 1, 2$.

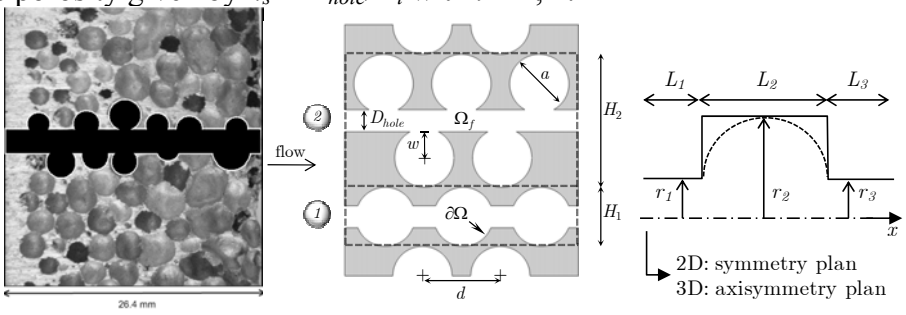

Figure 1. Example of a perforation through a real closed-cell aluminum foam sample (left). Two-dimensional model geometry of a perforated closed-cell metallic foam (center), showing two periodic unit cell (PUC) configurations: (1) lined-up, and (2) alternated.

2.2 Multi-scale acoustic properties of rigid porous media

The macroscopic description of long-wavelength acoustic propagation and dissipation phenomena through an inter-connected fluid filled rigid porous media may be modeled as an equivalent fluid [5] characterized by two complex frequency-dependent functions: the dynamic density $\rho_{eq}(\omega)$ which takes into account the visco-inertial interaction between the frame and the saturating fluid, and the dynamic bulk modulus $K_{eq}(\omega)$, which takes into account the thermal interaction. These dynamic functions can be respectively derived from macroscopic parameters using different semi-phenomenological models [6]-[7]. Johnson et al. [6] used four macroscopic parameters for modeling the visco-inertial interaction: the open porosity ϕ, the static airflow resistivity σ, the tortuosity α_∞, and their newly introduced viscous characteristic length Λ. Similarly, Champoux and Allard [7] introduced one additional macroscopic parameter for modeling the thermal interaction: the thermal characteristic length Λ'. In this work, for trend investigation purposes, the descriptions of the visco-inertial and thermal interactions between the rigid frame and saturating fluid are respectively restricted to the Johnson *et al.* [6] model, and the Champoux and Allard [7] model. In the following, the finite element analysis is used for solving the asymptotic low (steady Stokes) and high (electric) frequency viscous boundary value problems at the local scale for non trivial local geometries. Then, the macroscopic parameters can be extracted from the fields solving these two asymptotic behaviors. See for example Zhou and Sheng [8], Gasser *et al.*[9], Perrot *et al.* [10], Lee *et al.*[11] for a detailed description of this approach. Note that due to the boundary conditions applied on the geometry, the 2D-microstructural model shown in Fig. 1 might be seen as a series of slits. In the case of a perforated closed-cell metallic foam, the perforation is cylindrical and the pores are spherical. Consequently, axisymmetry seems more appropriate to represent the idealized micro-geometry even though it is not exact. Thus, simple analytical relationships enabling a 2D/3D correction factor are applied for the sake of result representativeness [3D macroscopic parameter (cylinder) / 2D macroscopic parameter (slits)] ([12]-[13]).

3. Results and discussion

Step by step, the influence of the microstructural parameters on the normal incidence sound absorption coefficient is now studied for three different porous configurations backed by a rigid termination. The configurations are illustrated in Fig. 2 and the microstructural parameters are those depicted in Fig. 1 (center). First, a single uniform tube of circular cross-section is analyzed to point out the existence of a perforation diameter maximizing the normal incidence sound absorption for a given sample length. Second, the case of a solid sample with several perforations of circular cross-section is examined to show the influence of the surface porosity or the perforation density. Third, the case of the perforated closed-cell metallic foam is numerically investigated using the multi-scale approach briefly described in the previous section. For this case, the effects of the relative position between the spherical pores and the perforations are first investigated, followed by the effects of the pore size. Finally, the 2D/3D analytical correction factors are used to transpose the 2D numerical results to 3D results with a view to compare normal incidence sound absorption predictions to impedance tube measurements. Note that for all the following simulations, dry air at standard conditions (18°C, 101.3 kPa) is considered.

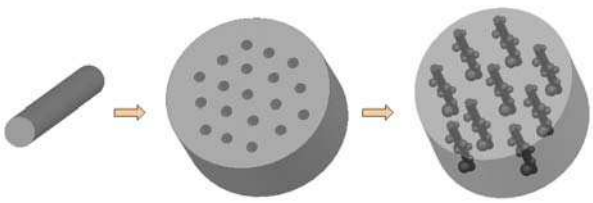

Figure 2. Main steps of the parametric study: (left) simple uniform tube of circular cross-section shape, (center) perforated solid, and (right) perforated closed-cell metallic foam.

3.1 Effects of the perforation diameter (Dhole)

3.1.1 Case of a single uniform tube (ϕ = 1)

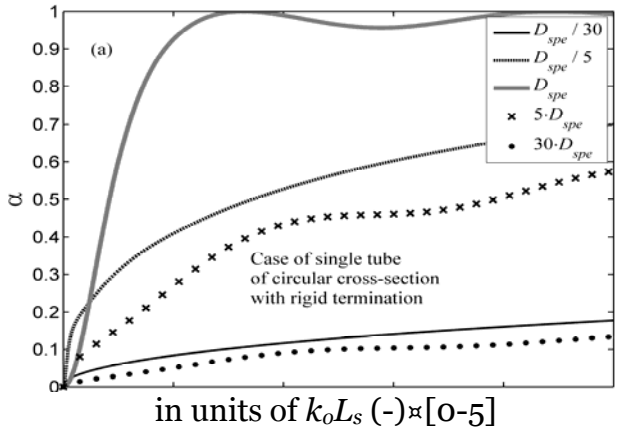

Figure 3. Sound absorption coefficient of a single cylinder of circular cross-section closed at the end.

The single uniform tube of circular cross-section shown in Fig. 4(a) is considered. The tube is closed at one end and has a diameter D_{hole} and a thickness L_s. Its macroscopic parameters are analytically obtained, and its normal incidence sound absorption computed.

Fig. 3 shows the influence of the perforation diameter on the sound absorption coefficient as a function of the dimensionless quantity k_0L_s, where k_o is the wave number in air. One can note that the overall sound absorption increases as the diameter increases until it reaches an *extremum* for a specific perforation diameter D_{spe}, and then starts decreasing. Here, D_{spe} is the diameter for which the sound absorption coefficient is equal to the unity at the first absorption peak (i.e., quarter wavelength absorption at approximately $k_0L_s = \pi/2$). It is worth mentioning that the diameters used to plot Fig. 3 are fractions or multiples of D_{spe} which depends on the thickness L_s as discussed below. Consequently, Fig. 3 is a normalized sound absorption graph that fits for all sizes of tubes of circular cross-section backed by a rigid termination.

3.1.2 Case of a perforated solid (ϕ < 1)

To illustrate the effects of the perforation density or porosity, the sound absorption coefficient of a perforated solid is plotted as a function of k_0L_s for four different porosities, see Fig. 4. For each porosity, sound absorption is computed for four different perforation diameters: $D_{spe}/30$, $D_{spe}/5$, D_{spe}, and $5D_{spe}$, where D_{spe} is the specific perforation diameter yielding 100% absorption at first peak. The specific resistance $(\sigma L_s)_{spe}$ corresponding to D_{spe} is also given for each porosity. It is obtained assuming $R_{hole} = D_{spe}/2$. Similarly, one can deduce the specific perforation density n_{spe} corresponding to each porosity.

In Fig. 4, one can first observe that for a low porosity, the absorption is very selective in terms of frequency and becomes less selective (i.e., bulk absorption) as the porosity increases. A typical selective case is a thin perforated solid with millimetric holes, and a typical bulk absorber case is a thin perforated solid with microperforations (or submillimetric holes). Now, if the curves maximizing the normal sound absorption coefficient for the four porosities are compared (thick lines), one can note that as ϕ (or n) increases, D_{spe} must be smaller to limit the decrease of $(\sigma L_s)_{spe}$ and to maintain 100% absorption at the first peak.

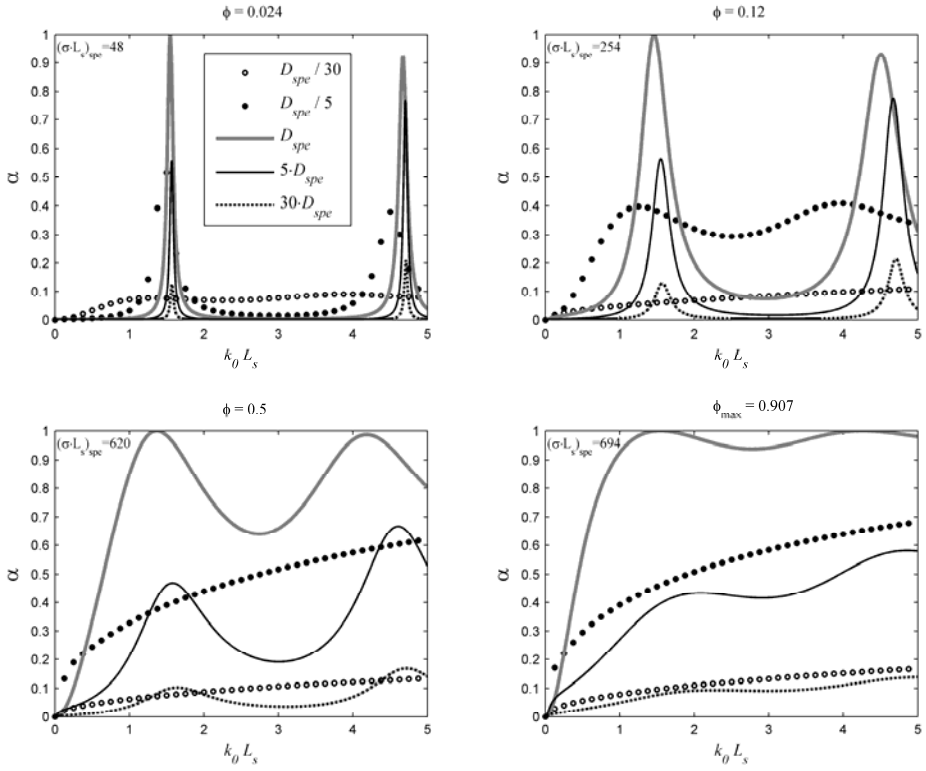

Figure 4. Sound absorption coefficient of a solid sample with cylindrical perforations of circular cross-section closed at the end for 4 different porosities.

3.2 Effects of the pore distribution (w, d)

The sound absorption behaviour of the perforated closed-cell foam sample depicted in Fig. 2(right) is now studied. Once again, the sample is backed by a rigid ending and its thickness is $L_s = 25$ mm. In what follows, three parametric studies are performed to evaluate how (1) the pore alignment, (2) the pore/perforation relative position w, and (3) the distance between pores d relate to the sound absorption spectrum in closed cell metallic foams.

To evaluate the effects of the alignment of the pores, two pore distribution patterns are compared: homogeneous and heterogeneous, see Fig. 5. The homogeneous distribution is similar to configuration 1 shown in Fig. 1(center-down). For the numerical simulations, $a = 1/10\,D_{hole}$ and $d = 3/2\,a$. Additionally, for the heterogeneous configuration, the pore/perforation relative position is randomly selected with the constraint that, in average, $\bar{w} = 0$ mm. Fig. 5 shows that both configurations yield close results in terms of sound absorption. Also, but not presented here, simulations on the alternated configuration of Fig. 1 (center-up) have shown that the alternated and line-up configurations yield the same results when $w = 0$ mm. Consequently, the homogeneous line-up configuration seems sufficient enough to represent the complexity of a heterogeneous pore distribution at macro-scale in terms of normal sound absorption coefficient when $\bar{w} = 0$ mm.

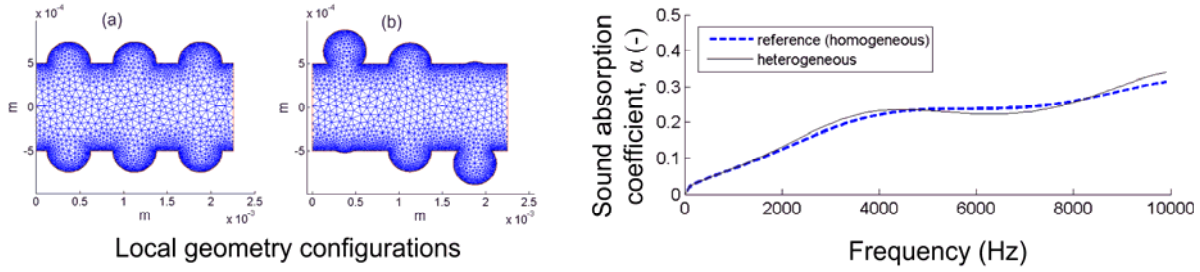

Figure 5. (a) Homogeneous vs (b) heterogeneous [left] pore distribution effect on the normal incidence sound absorption coefficient [right] of a perforated closed-cell metallic foam

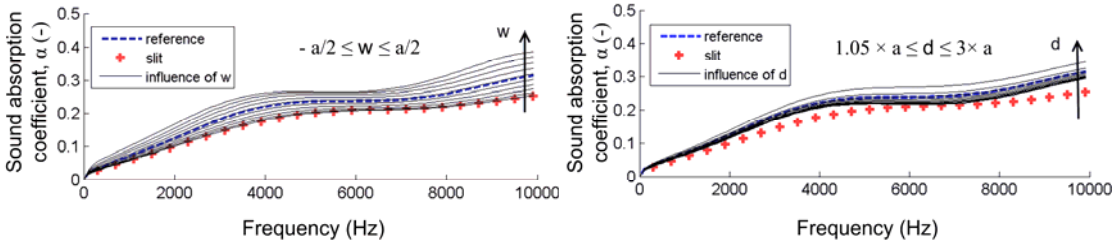

Figure 6. Pore/perforation relative position effect (w) [left], and inter-pore distance effect (d) [right] on the normal incidence sound absorption coefficient of a perforated closed-cell metallic foam.

The influence of d and w are now investigated. In this case, d and w are successively varied from the reference homogeneous configuration (D_{hole} = 1 mm, a = 1/10 D_{hole}, d = 1.5 a, w = 0 mm). Note again that for this reference configuration, simulation results showed that lined-up and alternated configurations yield identical results. The range of variation for d is from 1.05 a to 3 a, and the one for w is from -0.45 a (close to the single slit case of width D_{hole}) to 0.45 a. Following the proposed numerical procedure, the computed sound absorption predictions are presented in Figs. 6, respectively. The results are also compared to the sound absorption of a slit and to the one of the reference case. In the used range of variation around the reference configuration, d was found to have no significant effect on the normal incidence sound absorption behavior. Similarly, a variation of w has a limited impact on the sound absorption. However, contrary to d, w has lower and upper physical limits. The upper limit is when $w = a/2$ (i.e., perforation does not hit pores), and its lower limit is $w = -a/2$ (i.e., pores fall within the perforation) – the lower limit yields identical results to the single slit case. To conclude, the previous analysis has shown that the local geometry parameters governing the pore/perforation relative position do not have significant effects on the sound absorption behavior, at least in the studied range of variations.

3.3 Effects of the pore diameter (a)

Once the perforation diameter and the pore arrangement are established, the pore diameter can be studied with the 2D-model. The 3D analytical correction can then be used to estimate the influence of this parameter on the 3D model. Here, the pore diameter a varies between $D_{hole}/10$ and $2D_{hole}$. In the following simulations, the lined-up homogeneous configuration is used with D_{hole} = 1 mm, d = 1.5 a, w = 0 mm, and L_s = 25 mm. Fig. 7 shows the 3D results obtained. In Fig. 7(a), a maximum porosity is considered, which means that elementary cells are side by side. This fixes the perforation density. The results of the calculation are to be compared to the case of the single cylindrical tube (i.e., ϕ=1, Fig. 3). In Fig. 7(b), an intermediate porosity is fixed by considering a perforation density of n = 30 279 perforations/m², corresponding to 20 elementary cells on a 29-mm diameter sample. The results are to be compared to the case of a perforated solid of the same perforation density and diameter. For this latter case, ϕ=0.024 (Fig. 4). In conclusion, the previous analysis has shown that the results found for the perforated solids can also be used to investigate the sound absorption properties of perforated closed-cell foams. However, the effects of the local parameters (w, d, and a) have to be taken into account, at least the pore diameter as a first approximation.

3.4 Experimental comparison

The model does not aim at exactly quantifying the normal sound absorption coefficient of a perforated closed-cell metallic foam, but an experimental comparison would enable to confirm the validity of the previous trends by linking the above microstructure parameters to sound absorption properties. The real material is the closed-cell aluminum foam shown in Fig. 1. The sample has a 29-mm diameter and a 26.4-mm thickness. Fifteen perforations have been drilled through the total thickness; the perforation diameter is D_{hole} = 1 mm. The mean pore size obtained by simple image analysis is $a = 3.62 \pm 0.57$ mm. The sample was tested in a Bruel & Kjaer 4026 small impedance

tube over the frequency range 500-6000 Hz. The sound absorption coefficient is negligible for the entire frequency range before drilling. Two simulations have been achieved. The first is realized with the 2D model with pore diameter, perforation diameter, and number of perforations as input local geometry parameters. The lined-up configuration and the homogeneous pore distribution are considered with $d = 1.5a$ and $w = 0$ mm. The simulation results obtained for the macroscopic parameters of the perforated foam are the following: $\Phi = 0.284$, $\sigma = 8433$ Pa.s.m^{-2}, $\alpha_\infty = 5.54$, $\Lambda = 0.281$ mm, $\Lambda' = 1.504$ mm. Secondly, a 2-mm thick perforated plate is considered at the front face of the sample to account for the densified skin created during foaming, see Fig. 1(left). In this case, an added mass correction has to be taken into account [5]. For highly resistive backing materials, this correction is calculated as a dynamic equivalent tortuosity according to the method proposed by Atalla and Sgard [14]. The correlation is not perfect but the model is able to represent the main features of the experimental results despite all approximations – it is able to capture the prevailing dissipation phenomena, Fig. 8.

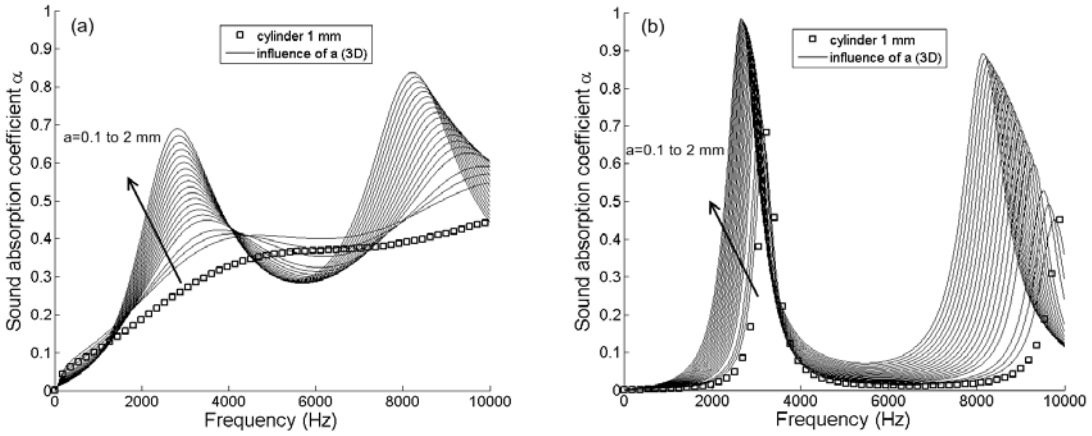

Figure 7. Influence of the pore diameter on the normal sound absorption coefficient. (a) Maximum porosity case. This configuration corresponds to assembling periodic unit cells (PUC) side by side. (b) Intermediate porosity case. This configuration corresponds to 20 PUC on a 29-mm diameter sample.

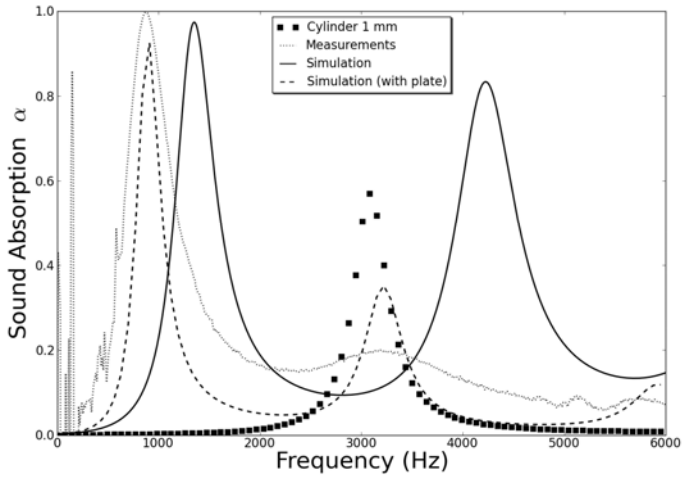

Figure 8. Normal incidence sound absorption coefficient of a real perforated closed-cell aluminum foam sample [see Fig. 1 (left)]. Measurements (dotted line) compared to numerical computations with (dashed line) and without (solid line) a perforated facing plate.

4. Concluding remarks

In this article, a microstructure based model was proposed to study the effects of perforations on the sound absorption of perforated closed-cell metallic foams. The theory of perforated solids was first revisited, then the given model was used to study the effects of the local geometry parameters on sound absorption of perforated closed cell metallic foams. From the obtained results and comparisons with perforated solids, one can draw the main outcomes as follows: (1) For the perforated solid, a specific perforation diameter was identified and derived as a function of the solid sample thickness, and further given in terms of a power-law relation as a design guide. (2) From this analysis, a practical formula to predict the specific resistance was subsequently proposed. (3) It was shown that the perforated closed-cell metallic foam shows a similar behavior than a perforated rigid solid; however its sound absorption may be strongly modulated by its local geometry parameters, most particularly by the interaction between perforation diameter and pore size. (4) Finally, it was shown that the pore size may have a strong effect on the sound absorption frequency selectivity. This can be of advantage during the metallic foam manufacturing process if the noise spectrum to be tackled is known.

5. Acknowledgement

This work was supported in part by grants-in-aid from N.S.E.R.C., C.Q.R.D.A., F.Q.R.N.T., REGAL., and Université Paris-Est Marne-la-Vallée.

REFERENCES

[1] M. F. Ashby, J. W. Hutchinson, and A. G. Evans, *Cellular Metals, A Design Guide* (Cambridge University Press, Cambridge, UK, 1998).

[2] T. J. Lu, A. Hess, and M. F. Ashby, "Sound absorption in metallic foams," *J. Appl. Phys.* **85**, 7528-7539 (1999).

[3] T. Miyoshi, M. Itoh, S. Akiyama, and A. Kitahara, "Alporas Aluminum Foam: Production Process, Properties, and Applications," *Advanced Engineering Materials* **2**, 179-183 (2000).

[4] T. J. Lu, F. Chen, and D. He. "Sound absorption of cellular metals with semiopen cells," *J. Acoust. Soc. Am.* **108**, 1697-1709 (2000).

[5] J. F. Allard and N. Atalla, *Propagation of sound in porous media. Modeling sound absorbing materials* – 2nd Ed. (Wiley, Chichester, UK, 2009).

[6] D. L. Johnson, J. Koplik, and R. Dashen, "Theory of dynamic permeability and tortuosity in fluid-saturated porous media, " *J. Fluid Mech*. **176**, 379-402 (1987).

[7] Y. Champoux and J. F. Allard, "Dynamic tortuosity and bulk modulus in air-saturated porous media," *J. Appl. Phys.* **70**, 1975-1979 (1991).

[8] M.-Y. Zhou and P. Sheng, "First-principles calculations of dynamic permeability in porous media," *Phys. Rev. B*, **39** (16), 12027-12039 (1989).

[9] S. Gasser, F. Paun, and Y. Bréchet, "Absorptive properties of rigid porous media: Application to face centered cubic sphere packing," *J. Acoust. Soc. Am.* **117**, 2090–2099 (2005).

[10] C. Perrot, F. Chevillotte, and R. Panneton, "Acoustic absorption calculation in irreducible porous media: A unified computational approach," *J. Acoust. Soc. Am.* **126**, 1862–1870 (2009).

[11] C.-Y. Lee, M. J. Leamy, and J. H. Nadler, "Bottom-up approach for microstructure optimization of sound absorbing materials," *J. Acoust. Soc. Am.* **124**, 940-948 (2008).

[12] Y. Champoux, "*Experimental study of acoustic behaviour of rigid porous media*," (in French) PhD Dissertation Thesis, Université de Sherbrooke (1991).

[13] Y. Champoux and M.R. Stinson, "On acoustical models for sound propagation in rigid frame porous materials and the influence of shape factors," *J. Acoust. Soc. Am.* **92**, 1120-1131 (1992).

[14] N. Atalla and F. Sgard, "Modeling of perforated plates and screens using rigid frame porous models," *J. Sound. Vib.* **303**, 195-208 (2007).